Random phase plates for beam smoothing on the Nova laser

S. N. Dixit, I. M. Thomas, B. W. Woods, A. J. Morgan, M. A. Henesian, P. J. Wegner, and H. T. Powell

We discuss the design and fabrication of 80-cm-diameter random phase plates for target-plane beam smoothing on the Nova laser. Random phase plates have been used in a variety of inertial confinement fusion target experiments, such as studying direct-drive hydrodynamic stability and producing spatially smooth x-ray backlighting sources. These phase plates were produced by using a novel sol-gel dip-coating technique developed by us. The sol-gel phase plates have a high optical damage threshold at the second- and third-harmonic wavelengths of the Nd:glass laser and have excellent optical performance.

Key words: Sol-gel coatings, random phase plates, binary-phase-only diffractive optical elements, laser beam smoothing.

1. Introduction

Directly driven targets for inertial confinement fusion (ICF) require laser beams with extremely smooth irradiance profiles to prevent hydrodynamic instabilities that destroy the spherical symmetry of the target during implosion.[1] Such instabilities can break up and mix together the target's wall and fuel material, preventing it from reaching the density and temperature required for fusion ignition. To avoid this, we must ensure that the rms intensity variations produced by the sum of all beams on target be no more than 1%.

However, the focal plane irradiance of Nd:glass ICF lasers typically has large-scale inhomogeneities produced by the aberrations in the beam. In high-power fusion laser systems such as Nova,[2] the fluence has to be maintained below a certain threshold to limit the optical damage to laser components. This is accomplished by expanding the beam cross section in successive amplifier stages as the beam energy is increased. This large cross section leads to beam aberrations from sources such as optical inhomogeneities, surface figure errors, and thermal nonuniformities. Additional aberrations are introduced when segmented optical components are used in the final amplifier stage. All these aberrations produce beams in large-scale ICF lasers that are many (approximately 20 to 50) times diffraction limited and thus highly modulated near the focus. Since smooth irradiation of the target is essential for its efficient compression, some method of beam smoothing is needed.

Techniques developed for smoothing laser beams can be divided into two categories: (1) spatial smoothing, in which the beam is broken up into a fine-scale spatial structure[3,4] that the target can potentially smooth by thermal conduction; (2) temporal smoothing,[5–10] in which the fine-scale structure is changed rapidly in time, leading to a beam with time-averaged smoothness. We do not discuss the temporal smoothing techniques further in this paper, although this method has also been implemented on Nova.[10] The spatial approach was first described by Kato et al.,[3] who used a bilevel random phase plate (RPP) (see the schematic diagram in Fig. 1) for ICF target experiments. RPP's have since been used in several laser fusion facilities, including Nova, for beam smoothing.

Fabrication of random phase plates for Nova posed several unique challenges. For operational convenience, we chose to make our RPP's at full aperture rather than segmented. This required fabrication of large-aperture (80-cm-diameter) phase plates.[11] Additionally, the phase-plate coating had to withstand high fluences in the visible (527 nm) and in the ultraviolet (351 nm), typically as high as 1.5 J/cm² in a ~1-ns pulse with as much as 2:1 intensity modulations. Previously, random phase plates have been fabricated by using the vapor deposition of a SiO₂ layer[11,12] or by using a photoresist coating[13] directly to
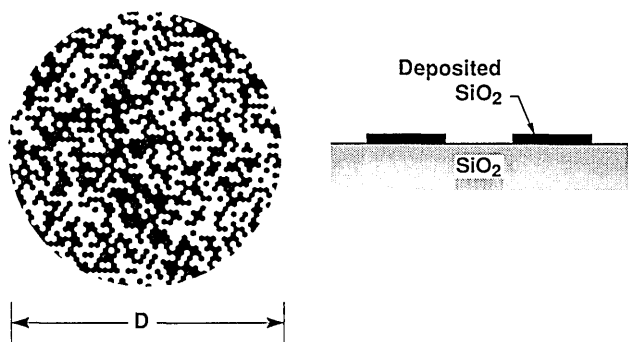
Fig. 1. Schematic layout of a random phase plate consisting of randomly distributed on–off phase-plate elements. A relative optical phase delay of π beween the on and the off elements is achieved by selectively depositing a thin SiO_2 layer, as shown on the right.

produce the relief pattern. Vapor-deposited coatings are expensive and difficult to produce at large apertures, while the photoresist coatings suffer from a low damage threshold in the ultraviolet.

Diffractive and holographic optical elements (DOE's and HOE's) such as lenslet arrays, binary- and/or continuous-phase screens, and gratings are being used in applications such as micro-optical chips, beam samplers and beam combiners, fan-in/fan-out-type beam couplers, and interconnects.[14] The principal differences between these integrated-optical elements and the phase plates used in fusion applications are the size (small for DOE's and HOE's and large for RPP's), the wavelength of use (IR for the former while visible-to-UV for the latter), and irradiation fluences (low for DOE's and HOE's and high for RPP's). These differences make the standard fabrication procedures for DOE's and HOE's that use photoresist and e-beam or ion-etching techniques impractical and/or expensive for fabrication of large-aperture high-damage-threshold RPP's for use at the visible and/or ultraviolet wavelengths.

We have developed a novel sol-gel process for fabricating bilevel phase relief structures.[15] The sol-gel RPP's were prepared by selectively etching away areas of a sol-gel coating layer. The sol-gel coating process is similar to that used in preparing the antireflection (AR) coatings[16] except that a polymeric sol-gel solution is used in RPP fabrication, whereas a colloidal sol-gel suspension is used in AR coatings. This procedure is easily scalable to large-aperture substrates and yields high-quality products with excellent optical performance and a high optical damage threshold. To date, we have fabricated several bilevel RPP's of different aperture and element sizes for use in infrared, visible, and ultraviolet wavelengths. Fabrication of DOE's with a sol-gel molding process has been reported recently.[17] Our process differs from this in that we deposit a sol-gel layer on a substrate and then etch the relief pattern in it. Our procedure is easily scalable to large apertures.

The details of the fabrication process are described in Section 3 after a brief discussion of the characteris-

tics of the random phase plates in Section 2. Characterization of the RPP's so produced, along with their performance on the Nova laser system, are discussed in Section 4. A summary and conclusions follow in Section 5.

2. Theory

This section briefly describes the characteristics of the focal-plane intensity distribution that results from the focusing of light through a bilevel RPP. These characteristics, together with the target-size specificiations, guide the design of the RPP's. As shown in Fig. 1, a typical RPP used for ICF studies consists of a contiguous layout of regularly spaced phase-plate elements randomly selected to be either on or off; the on elements impose a π-phase shift on the beam relative to the off elements. Commonly used phase-plate-element shapes consist of hexagons, rectangles, and squares. As shown below, the far-field distributions of these shapes can be described analytically. Although, in principle, any close-packed pattern can be used in designing a phase plate, we restrict ourselves to hexagonal- and rectangular-shaped elements, with square elements viewed as a special case of rectangular elements.

The electric-field distribution $E(\rho, f)$ at the focal plane of a lens can be written as a Fourier transform of the incident field $E_0(\rho', 0)$[18]:

$$E(\rho, f) = \frac{-i}{\lambda f} \exp\left(\frac{\pi i \rho^2}{\lambda f}\right)$$
$$\times \int_{\text{aperture}} d\rho' E_0(\rho', 0) \exp\left(\frac{-2\pi i \rho \cdot \rho'}{\lambda f}\right), \quad (1)$$

where $\rho'[= (x', y')]$ and $\rho [= (x, y)]$ are, respectively, the transverse coordinates in the input and the focal plane, λ is the laser wavelength, and f is the lens focal length. The incident field $E_0(\rho', 0)$ inside the integrand in Eq. (1) includes the phase shifts introduced by the random phase plate and any other phase aberrations present in the beam. In Eq. (1) we assume that the laser beam is uniformly polarized. If the incident laser beam is assumed to be constant over each individual phase-plate element, the integral in Eq. (1) can be rewritten as a sum of subintegrals over the individual phase-plate elements:

$$E(\rho, f) = \exp\left(\frac{\pi i \rho^2}{\lambda f}\right) S(x, y, f)$$
$$\times \sum_{\text{elements } j} E_0(\rho_j', 0) \exp\left(\frac{-2\pi i \rho \cdot \rho_j'}{\lambda f}\right) \quad (2)$$

where $\rho_j' = (x_j', y_j')$ denotes the center of the jth phase-plate element and

$$S(x, y, f) = \frac{-i}{\lambda f} \int_{\text{phase-plate element}} d\rho' \exp\left(\frac{-2\pi i \rho \cdot \rho'}{\lambda f}\right) \quad (3)$$

denotes the far-field pattern of a single phase-plate

element. Thus the far-field intensity pattern of an RPP has an overall envelope produced by the diffraction pattern of a single element that is modulated by a fine-scale interference pattern caused by contributions from various phase-plate elements.

We first discuss the characteristics of the overall intensity envelope. The far-field patterns of rectangular and circular apertures are well known.[19] For example, $S(x, y, f)$ for a rectangular aperture of sides a and b is given by

$$S(x, y, f) = \frac{-i}{\lambda f} ab \operatorname{sinc}\left(\frac{\pi a x}{\lambda f}\right) \operatorname{sinc}\left(\frac{\pi b y}{\lambda f}\right), \quad (4)$$

where

$$\operatorname{sinc}(x) = \sin(x)/x.$$

The central maximum of this pattern contains 81.5% of the total energy. On the other hand, the Airy pattern generated by a circular aperture contains slightly more (84% of the total) energy in its central maximum. As we show below, a regular hexagonal aperture also concentrates, in the central maximum, 84% (equal to that of a circular aperture) of the total energy. For this reason, we choose to fabricate RPP's mainly with hexagonal-shaped elements.

General closed-form (but complicated) expressions can be developed for the far-field patterns of polygons. Diffraction properties of polygonal apertures have been numerically and experimentally investigated.[20] However, to the best of our knowledge, the detailed analytical expression for general hexagons given below has not been published before. We consider a stretched hexagonal shape, characterized by three distances h_1, h_2, and h_3, as indicated in Fig. 2. A regular hexagonal aperture is characterized by $h_3 = 2h_2 = 2h_1/\sqrt{3}$, while $h_3 = h_2$ leads to a rectangular aperture. $S(x, y, f)$ for such a shape can be written as

$$
\begin{aligned}
S(x, y, f) = \frac{-iA}{\lambda f} &\left(\frac{2h_2}{h_2 + h_3} \operatorname{sinc}\left(\frac{\pi x h_1}{\lambda f}\right) \operatorname{sinc}\left(\frac{\pi y h_2}{\lambda f}\right) \right. \\
&+ \frac{h_3 - h_2}{h_3 + h_2} \frac{\lambda f}{\pi x h_1} \left\{ \operatorname{sinc}\left[\frac{\pi x h_1}{2\lambda f} + \frac{\pi y (h_3 - h_2)}{2\lambda f} \right] \right. \\
&\times \sin\left[\frac{\pi x h_1}{2\lambda f} - \frac{\pi y (h_3 + h_2)}{2\lambda f} \right] \\
&+ \operatorname{sinc}\left[\frac{\pi x h_1}{2\lambda f} - \frac{\pi y (h_3 - h_2)}{2\lambda f} \right] \\
&\left. \left. \times \sin\left[\frac{\pi x h_1}{2\lambda f} + \frac{\pi y (h_3 + h_2)}{2\lambda f} \right] \right\} \right), \quad (5)
\end{aligned}
$$

where

$$A = \frac{h_1(h_2 + h_3)}{2} \quad (6)$$

denotes the area of the hexagon. Although this expression appears algebraically complex, it has the
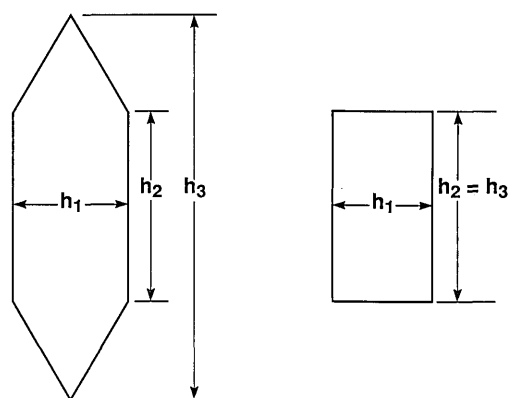

Fig. 2. Parametrization of a stretched hexagonal aperture. On the right, a rectangular aperture is shown as a special case of the stretched hexagonal aperture.

expected physical properties. For example, setting $h_3 = h_2$ in Eq. (5), one recovers the familiar expression for the far-field pattern of a rectangular aperture given in Eq. (4).

The calculated far-field intensity patterns $[|S(x, y, f)|^2]$ for a regular hexagonal and for a stretched hexagonal phase-plate element are shown in Fig. 3. The symmetries corresponding to the hexagonal aperture are quite apparent in this figure. To under-
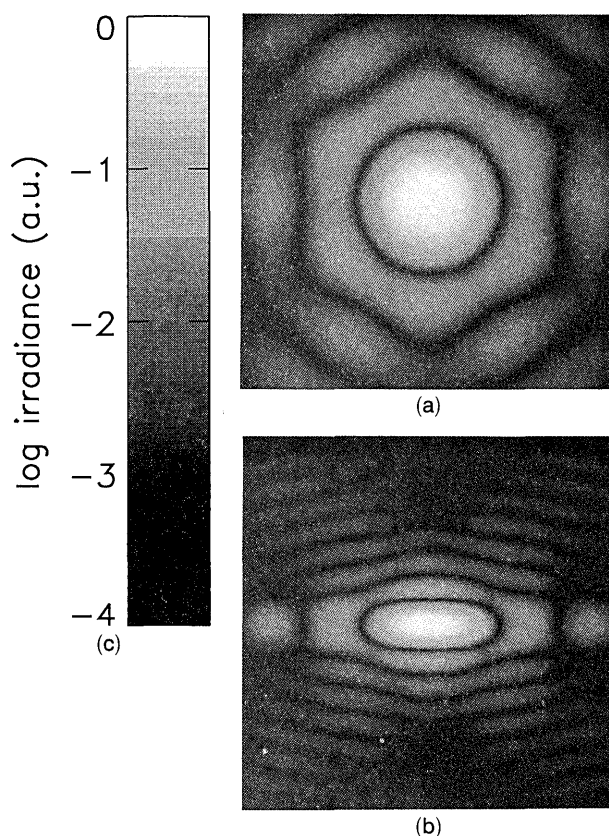

Fig. 3. Far-field diffraction patterns $|S(x, y, f)|^2$ [from Eq. (5)] for (a) a regular hexagonal aperture ($h_3 = 2h_2 = 2h_1/\sqrt{3}$) and (b) for a stretched hexagonal aperture with $h_2 = 2h_1$ and $h_3 = 3h_1$. The transverse distances for both cases are in units of $\lambda f/h_1$, and the peak intensity is normalized to 1.

stand the spatial extent of the central maximum, we examine the far-field expression in Eq. (5) along the x ($y = 0$) and y ($x = 0$) axes. $S(x, 0, f)$ and $S(0, y, f)$ are obtained by setting the appropriate limits in Eq. (5) and can be written as

$$
\begin{aligned}
&S(x, 0, f) \\
&= \frac{-iA}{\lambda f}\left[\frac{2h_2}{h_2 + h_3}\operatorname{sinc}\left(\frac{\pi x h_1}{\lambda f}\right) + \frac{(h_3 - h_2)}{h_2 + h_3}\operatorname{sinc}^2\left(\frac{\pi x h_1}{2\lambda f}\right)\right],
\end{aligned}
$$

(7a)

$$
\begin{aligned}
&S(0, y, f) \\
&= \frac{-iA}{\lambda f}\left\{\operatorname{sinc}\left[\frac{\pi y(h_3 - h_2)}{2\lambda f}\right]\operatorname{sinc}\left[\frac{\pi y(h_3 + h_2)}{2\lambda f}\right]\right\}.
\end{aligned}
$$

(7b)

Particular limits of Eqs. (7a) and (7b) for a regular hexagonal aperture agree with the expressions given elsewhere.[12] Equation (7b) implies that the first minimum occurs at

$$
y_{\min} = \pm\frac{2\lambda f}{(h_3 + h_2)}.
$$

(8)

Interestingly, the position of the minimum in the y direction is independent of the hexagonal extent (h_1) in the x direction. The minima in the x direction are given by the zeros of $S(x, 0, f)$. Equation (7a) implies that the first minimum occurs somewhere between $\lambda f/h_1$ and $2\lambda f/h_1$ with the actual position dependent on the ratio h_3/h_2. For $h_3/h_2 = 1$ the first minimum occurs at $\lambda f/h_1$ (rectangular case), and for $h_3/h_2 \to \infty$, the minimum occurs at $2\lambda f/h_1$. Figure 4 illustrates the dependence of the position of the first minimum on the ratio h_3/h_2. The dependence of the minima in the x direction on the dimensions h_2 and h_3 in the y direction reflects the consequences of the hexagonal shape of the aperture.

Note the near-circular symmetry of the central maximum in the far field of a regular hexagon shown in Fig. 3(a). Although not obvious from Eq. (5), numerical calculations indicate that the intensity pattern of a regular hexagon within the central maximum is practically identical to the Airy pattern of an equal-area circular aperture. The diameter of such an equivalent circular aperture is determined by
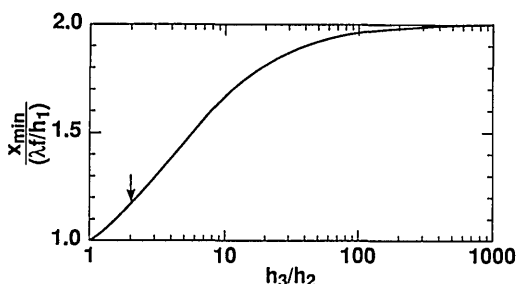

Fig. 4. Dependence of the position of the first minimum in the x direction on the ratio h_3/h_2. The arrow at $h_3 = 2h_2$ corresponds to the regular hexagonal case.

the equality[12]

$$
\frac{\pi}{4}\tilde{d}^2 = \frac{\sqrt{3}}{2}h_1{}^2,
$$

and the first minimum occurs at

$$
r_{\min} = 1.22\frac{\lambda f}{\tilde{d}} = 1.22\left(\frac{\pi}{2\sqrt{3}}\right)^{1/2}\frac{\lambda f}{h_1} \approx 1.16\frac{\lambda f}{h_1}.
$$

(9)

This position is indicated by the arrow in Fig. 4 (at $h_3/h_2 = 2$, corresponding to a regular hexagon). As far as the central maximum is considered, the hexagonal aperture appears similar to a circular aperture. Integration of the far-field intensity distribution indicates that the central maximum contains 84% of the incident energy.

Returning to the far field of the entire phase plate, we see that Eq. (2) simplifies, for a uniform input intensity beam, to

$$
\begin{aligned}
E(\rho, f) &= \exp\left(\frac{\pi i\rho^2}{\lambda f}\right)E_0 S(x, y, f) \\
&\times \sum_{\text{elements } j}\exp\left[\frac{-2\pi i(xx_j' + yy_j')}{\lambda f} + \phi_j\right],
\end{aligned}
$$

(10)

where E_0 denotes the incident-field amplitude and ϕ_j is the phase factor at the jth phase-plate element imposed by the RPP plus any relative phase inherent in the beam. For bilevel phase plates the RPP contribution to ϕ_j has only two values, 0 or π. The far-field intensity distribution is given by

$$
\begin{aligned}
I(x, y, f) &= I_0 |S(x, y, f)|^2 \\
&\times \left|\sum_{\text{elements } j}\exp\left[\frac{-2\pi i(xx_j' + yy_j')}{\lambda f} + \phi_j\right]\right|^2,
\end{aligned}
$$

(11)

with I_0 denoting the input intensity.

Although the contribution to ϕ_j from the RPP has only two values, the net phases of the contributions from the various RPP elements are substantially randomized by the combination of the rapidly varying phase term (i.e., the Fourier kernel) and the randomly occurring phase jumps. This addition of a large number of equal-magnitude random-phase components in Eq. (10) produces a speckle pattern of intensities. From the fastest varying phase term in Eq. (10), one can see that the characteristic size of the speckle is of the order of $2f\lambda/D$, where D is the diameter of the full aperture. This is ~ 5 μm in the target plane for the Nova beam ($\lambda = 527$ nm, $f = 3$ m, and $D = 70$ cm). These features are illustrated in Fig. 5(a), in which we present a 200-μm-long line scan through a calculated speckle pattern near the maximum of the envelope function. The phase-plate elements were regular hexagons with $h_1 = 3.5$ mm. Other parameters were as mentioned above for the Nova beam. The fine-scale speckle of ~ 5-μm size is
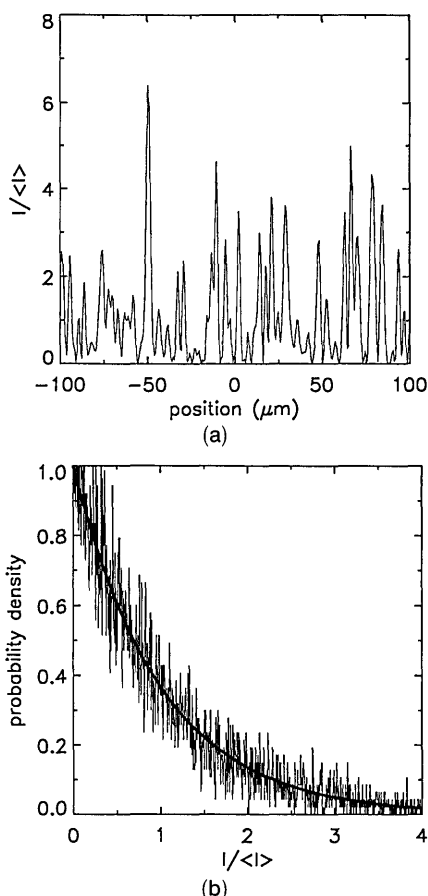
Fig. 5. (a) Line scan through a calculated speckle pattern generated by the random phase plate. See the text for the parameters used in the calculation. (b) Histogram of the intensity distribution for the calculated speckle pattern over a 200 μm × 20 μm area is compared with the negative exponential probability distribution. The maximum on the abscissa is truncated at 4.0 for clarity. Intensity peaks much higher than 4 times the average are commonly observed.

clearly visible. A well-known characteristic of a speckle pattern is that the probability density of intensity follows a negative exponential distribution.[21] In Fig. 5(b) the histogram of the intensities from the simulations of the speckle pattern over a 200-μm × 20-μm-wide region near the maximum of the envelope function is compared with a negative exponential probability distribution. Good agreement between these two distributions confirms the characteristic property of the speckle.

It is easy to see from Eq. (10) that no x_j- and y_j-dependent randomization in phase occurs exactly on axis $(x = y = 0)$. This can lead to a coherent spike on axis. For a uniphase incident beam the height of the coherent spike relative to the average intensity $[= NI_0$, defined as the incoherent summation in Eq. (11)] is given by

$$\frac{\text{spike}}{\text{background}} = \frac{1}{N} |N_+ + N_- \exp(i\delta)|^2, \quad (12)$$

where N_+ and N_- denote the number of on elements

and off elements, respectively, with a relative phase difference δ and $N = N_+ + N_-$ is the total number of phase-plate elements. We see that the coherent spike can arise either from a mismatch in the number of on and off elements $(N_+ \neq N_-)$ and/or from δ being different from π. For RPP designs with $N_+ \approx N_-$, Eq. (12) simplifies to

$$\frac{\text{spike}}{\text{background}} = N \cos^2\left(\frac{\delta}{2}\right). \quad (13)$$

Figure 6 illustrates the dependence of the coherent-spike-to-background ratio on δ for different values of N. It is clear that, for RPP's containing a large number of phase-plate elements, suppression of the coherent spike places stringent requirements on the relative phase difference δ. On the other hand, this requirement is relaxed considerably when there are large inherent phase variations present in the beam. This is discussed further in Section 4 in connection with the phase-plate performance on the Nova beam. The coherent spike can also be eliminated by operating in a plane that is several Rayleigh ranges for the full beam $(\sim 8\lambda f^2/D^2)$ away from focus. In this case, the residual phase curvature (defocusing aberrations) suppresses the coherent addition of the electric phasors in Eq. (12).

3. Fabrication of Sol-Gel Phase Plates

This section describes our sol-gel RPP fabrication procedure. Conventionally, RPP's are prepared by evaporating silicon dioxide (SiO_2) in a vacuum onto a substrate that has been coated with photoresist.[11,12]
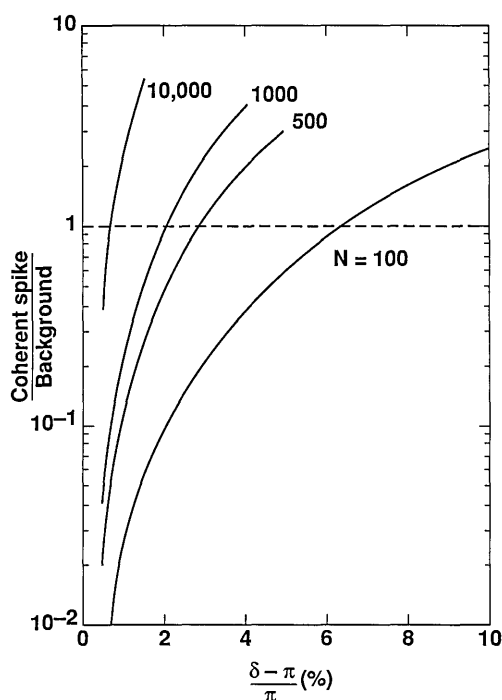

Fig. 6. Dependence of the coherence spike on the number of coherently illuminated phase-plate elements N and on the error in the relative optical phase difference δ. Desirable phase plates would have a coherent-spike-to-background ratio near or below unity.

A suitable random design is patterned with a photo mask in the photoresist. Development of the exposed photoresist leaves bare and coated areas on the substrate. A uniform layer of SiO$_2$ of precise thickness is then deposited upon the substrate by using conventional vapor-deposition methods. The photoresist is then chemically removed together with the evaporated SiO$_2$ coating over these regions, leaving a pattern of SiO$_2$ pixels that correspond to the positive of the photomask. This is the phase plate. It is important in this process to have good control over the thickness of the deposited silica and to ensure that the bare areas on the substrate (following the photoresist development) are extremely clean before SiO$_2$ deposition in order that a sharp pattern can be obtained. Originally, we fabricated two 80-cm-diameter phase plates by this procedure when we worked with Spectra Physics Optics Corporation. However, we found that the process was expensive and produced RPP's having moderate damage thresholds (~ 8 J/cm^2 at 532 nm and <4 J/cm^2 at 351 nm for 10-ns pulses).

We developed a sol-gel process to fabricate the random phase plates. The main steps in this procedure are schematically illustrated in Fig. 7. This process differs from the vapor-deposition method described above in that the whole substrate is first coated with a sol-gel silica layer, which is then selectively etched off through a patterned photoresist layer that is deposited over the silica coating. The silica under the coated areas is protected from attack by the HF etchant, which removes the bare or unprotected silica. Removal of the resist then gives the patterned substrate, the pattern being the positive of the original one on the photoresist and a negative of the photo mask. Details of the fabrication process are described below.

A. Silica-Coating Deposition

The first step in the sol-gel RPP fabrication consists of depositing a uniform layer of silica on the substrate.
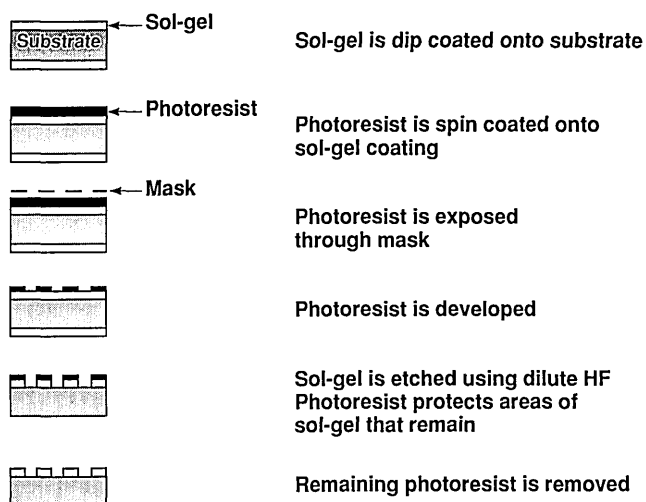

Fig. 7. Schematic illustration of the sol-gel phase-plate fabrication procedure.

We deposited the coating by dipping the substrates in a hydrolysed ethyl silicate solution. The preparation of silica coatings from solutions of hydrolysed ethyl silicate is well known. An excellent summary with all the variations is given by Brinker and Scherer.[22] Depending on reaction and cure conditions, coatings can range from quite porous to nearly fully dense. The dense films, which have the greatest mechanical strength, are normally obtained by using acid-catalyzed solutions and by heating the substrate after the coating has air dried. We found that, by exposing air-dried silica coatings made from an acid-catalyzed solution to ammonia and water vapor for at least 24 h at room temperature, we could obtain coatings that were $\sim 95\%$ dense. This eliminated the need for additional heating. Exposure to ammonia/water vapor was carried out by enclosing the sample in a closed container that contained a beaker of concentrated ammonium hydroxide solution at room temperature. These coatings remained stable and unchanged for a long period at room temperature, could be handled and cleaned as conventional optics, and could also be etched in dilute hydrofluoric acid at a much faster rate than a fully dense substrate.

We have made phase plates of 15–80-cm diameter and found that these could be conventionally dip coated from a 200-L tank of silicate solution. A similar dip-coating method has been used extensively in our laboratory to prepare sol-gel AR coatings.[16] About 200 L of hydrolysed ethyl silicate solution containing the equivalent of 10% SiO$_2$ was prepared directly in the coating tank as follows. Tetraethylsilicate (25 kg) was solvated in anhydrous ethyl alcohol (189 kg), and diluted hydrochloric acid (10 g in 19.4 kg of water) was slowly added. The solution was continuously recirculated through a 1-μm cartridge filter, which also helped to mix the reagents. A slight exotherm indicated that hydrolysis was proceeding. After 30 min., more tetraethylsilicate (31 kg) was slowly added over a period of another 30 min. Recirculation and filtration was continued for an additional 60 min. The solution was then left sealed in the tank at room temperature for a period of at least 2 weeks prior to use.

Samples of 5–80-cm diameter were dip coated in the silicate solution in a clean environment at withdrawal rates varying from 4 to 8 cm/min., depending on the thickness requirement. Since the viscosity of the sol-gel solution changes over a period of a few weeks, witness samples (up to 15-cm-diameter BK7) were pulled each time to determine the required rates. Coated samples were air dried at room temperature for 6 h and then recoated if necessary. If not recoated, they were placed in a closed container over concentrated ammonium hydroxide solution for a minimum of 24 h. Recoated samples were treated with ammonia vapor only after the final coat.

The thickness and the refractive index of the sol-gel coating were determined by measuring the transmission of the coated part in a spectrophotometer. The

index of refraction of the coating can be calculated by using[23]

$$n_c = n_s \frac{(1 + \sqrt{R})}{(1 - \sqrt{R})}, \qquad (14)$$

where n_c is the index of refraction of the coating, n_s is the index of refraction of the substrate, and R is the reflectivity at one of the maxima or minima of the transmission curve, depending on whether $n_c < n_s$ or $n_c > n_s$. Figure 8 shows a typical scan of the transmission through the sample. The measured refractive index of the coating was 1.440 ± 0.005 at 527 nm. Because the refractive index of the sol-gel silica coating was lower than that of the silica substrate (1.46 at 527 nm), it was slightly antireflective. The optical thickness can be determined from the positions of the transmission extrema by using the equation

$$n_c t = \frac{\lambda_p}{4} (2K + 1), \qquad (15)$$

where t is the coating thickness, λ_p is the wavelength of an extrema of the transmission curve, and $K = 1, 2, 3, \ldots$. These equations are applicable only if the film thickness is at least equal to $\lambda_p/4$.

The optical path difference (OPD), at normal incidence, between the coated and the uncoated regions, is given by

$$\text{OPD} = (n_c - 1)t. \qquad (16)$$

As discussed in Section 2, the suppression of the on-axis coherent spike requires that the OPD be fairly close to $\lambda/2$. Samples were usually prepared for use at either 351 or 527 nm. Based on the measured value of the refractive index (1.440 ± 0.005), these samples therefore required thicknesses of 394–403
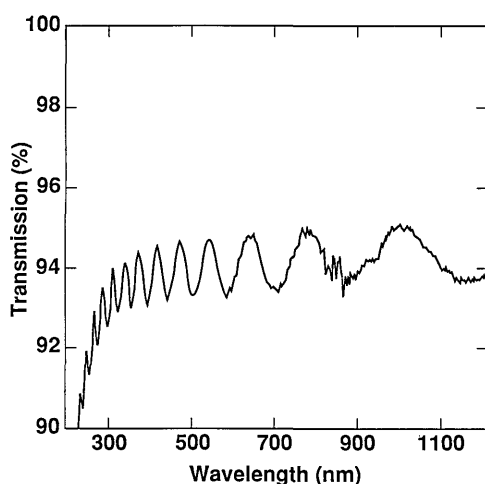

Fig. 8. Measurement of the transmission through the sol-gel coating as a function of the wavelength. From the positions of the extrema in transmission and the amount of transmission at these positions, the coating thickness and its refractive index can be calculated as discussed in the text.

nm and 592–606 nm, respectively. The former could be prepared with a single coating, but the latter required two coatings. For samples requiring a single coating (UV applications) the pull rate was predetermined based on the required thickness and the sol-gel viscosity. On the other hand, for coatings requiring multiple dips, pull rates for later dips were suitably adjusted to achieve the required thicknesses.

B. Photoresist Coating, Development, and Etching

The next step in the RPP fabrication is the selective etching away of the silica coating. This was accomplished by depositing a layer of photoresist, exposing it through a suitable photomask, developing it, and finally etching away the sol-gel coating from the unprotected areas on the substrate. Although sol-gel silica coatings could be easily deposited, there were several potential problems that had to be solved in order to obtain high-quality phase plates. We had to be certain that the remaining resist pattern after development would protect the underlying silica layer from attack by the etchant and also that we could use an etchant concentration that would rapidly remove the slightly porous sol-gel silica and not affect either the photoresist layer or the dense underlying silica substrate. We also hoped that there would not be much undercutting during the etch in order to get sharply defined pixels.

Because of the high cost of photoresist, we used spin coating rather than dip coating for application of the resist to the silicate-coated substrate. We found that a coupling agent was necessary to ensure good adhesion of the resist of the silicate. A thin layer of the coupling agent (Shipley C-50, hexamethyldisilazane in 2-ethoxyethyl acetate) was first applied to the sample at slow speed and permitted to dry for ~ 60 s. This was then followed by the photoresist (Shipley 1400-27), which was spun until dry to the touch. Coating speeds varied from approximately 1500 rpm for the small 5-cm samples to 300 rpm for the large 80-cm samples. The coated samples were finally dried in a forced-air environment at 30 °C for at least 16 h. The thickness of the photoresist coat was 2–2.5 μm.

The photoresist was then exposed through a photomask containing a black-and-white image of a random pattern of interlocking hexagonal, square, or rectangular phase-plate elements, as shown in Fig. 1. The mask was generated on a photographic film by using a computer-controlled light pen stage with 25-μm resolution. A random layout of the on–off elements was selected. Recently, Epstein and Skupsky have discussed[24] more sophisticated, quasi-random RPP element patterns. The RPP mask was placed in contact with the resist and illuminated with UV light from germicidal lamps for ~ 70 min. The resist was then developed by using a dilute base (Shipley 354).

After development, we found that the unprotected silica could be readily removed by etching in 1% aqueous HF solution for 4 min. There was little

effect on the substrate by the etchant solution in this period of time, and photoresist-coated silicate areas remained unetched. Sharp distinct silica pixels were obtained on the substrate after the subsequent removal of the remaining photoresist. Finally, the phase plates were AR coated with sol-gel porous silica[16] prior to installation in the laser system.

4. Phase-Plate Characterization and Performance

A. Far-Field Measurement

The RPP's were tested to find out how closely we had come to making a $\lambda/2$ optical path difference between the on and the off elements. In an off-line test (see Ref. 11 for details) we placed the RPP in a 30-cm-diameter near-diffraction-limited beam from a cw argon-ion laser and recorded the far-field image obtained with a 3-m focal-length lens either on film or on a Big Sky video beam profiler. The argon-ion laser can be operated at either the 529- or 351-nm lines, which are near the operating wavelengths of the Nova laser at the second and the third harmonics of Nd:YLF (526.5 and 351 nm). The film image was digitized with a Perkin Elmer densitometer and processed on computer. The density versus exposure response for the film was deduced by analyzing the image of a precise intensity wedge on the film.

The far-field image of an RPP composed of 1.3-mm square elements is shown in Fig. 9(a). The overall envelope corresponding to the far-field diffraction pattern of a single phase-plate element as well as the fine-scale speckle are visible. The exposure at the center portion of this image is saturated in order to display the secondary maxima in the pattern. The line scan [Fig. 9(b)] through the center of a processed unsaturated image indicates a nearly 230-to-1 coherent spike on axis. Based on the number of coherently illuminated elements ($\sim$40,000 in a 30-cm-diameter beam), Eq. (13) implies an OPD errror of $\sim$5%. This is in reasonable agreement with topographic measurements of step height discussed below. A few percent OPD error would lead to an even higher coherent spike if the full 80-cm-aperture RPP were illuminated with a coherent beam. However, as discussed in Subsection 4.D below, beam aberrations on Nova reduce the effective coherence zone size and thus minimize and in most cases eliminate the coherent spike. Thus a few percent OPD error is tolerable for RPP's used on Nova.

Figure 9(a) also shows a series of regularly spaced sharp spikes located at the minima of the far-field pattern. These arise from the Bragg diffraction from the (finite-width) boundaries between the on–off regions. The regularity and the sharpness of these grating spikes reflects the regularity of the edges on the RPP. When we roughened the phase-plate-element edges by treating them with a mild acid, the grating spikes disappeared, thus verifying that these spikes were indeed originating from the diffraction at the edges. We have observed the grating spikes on almost all of our RPP's in off-line measurements.
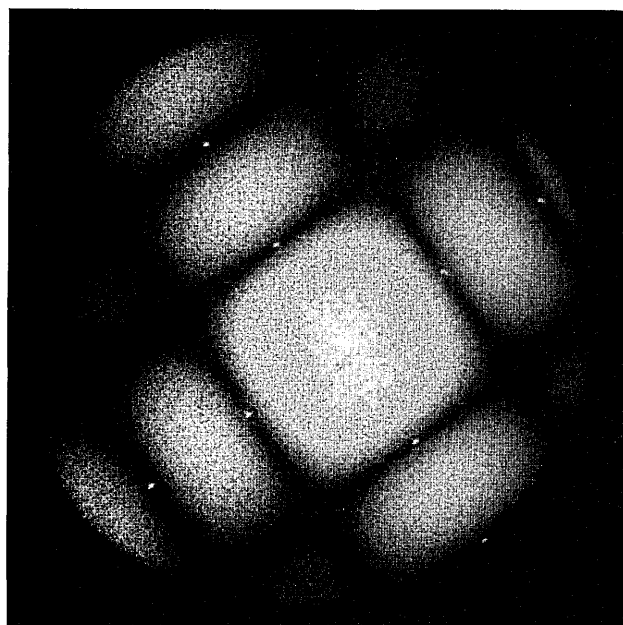
(a)
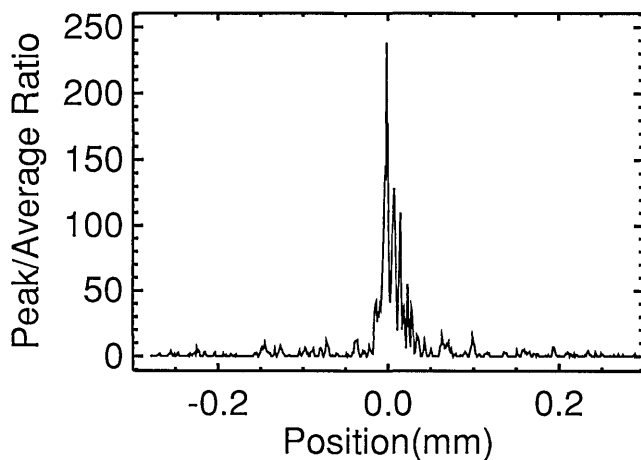
(b)

Fig. 9. (a) Far-field film image of a coherently illuminated 30-cm-diameter random phase plate composed of 1.3-mm square elements. The light wavelength is 351 nm, and the focal length of the lens is 3 m. (b) Line scan through a central portion of an unsaturated image similar to that shown in (a).

As with the coherent spike, the grating spikes are also diffused or eliminated by beam aberrations.

B. Topography

The thickness of the coating and the edge definition of the phase elements were determined by several methods. One method used a high-resolution phase-measuring laser interferometric microscope (Zygo Maxim●3D). The spatial resolution of the instrument with a 40× objective is 1 μm with a vertical accuracy of 6 nm. A second method used a portable atomic force microscope. This instrument can scan areas as large as 100 μm × 100 μm and can have vertical resolution on the atomic scale. Typical stylus pressures applied to the part are of the order of 10^{-8} N. Both measurement methods agreed as to
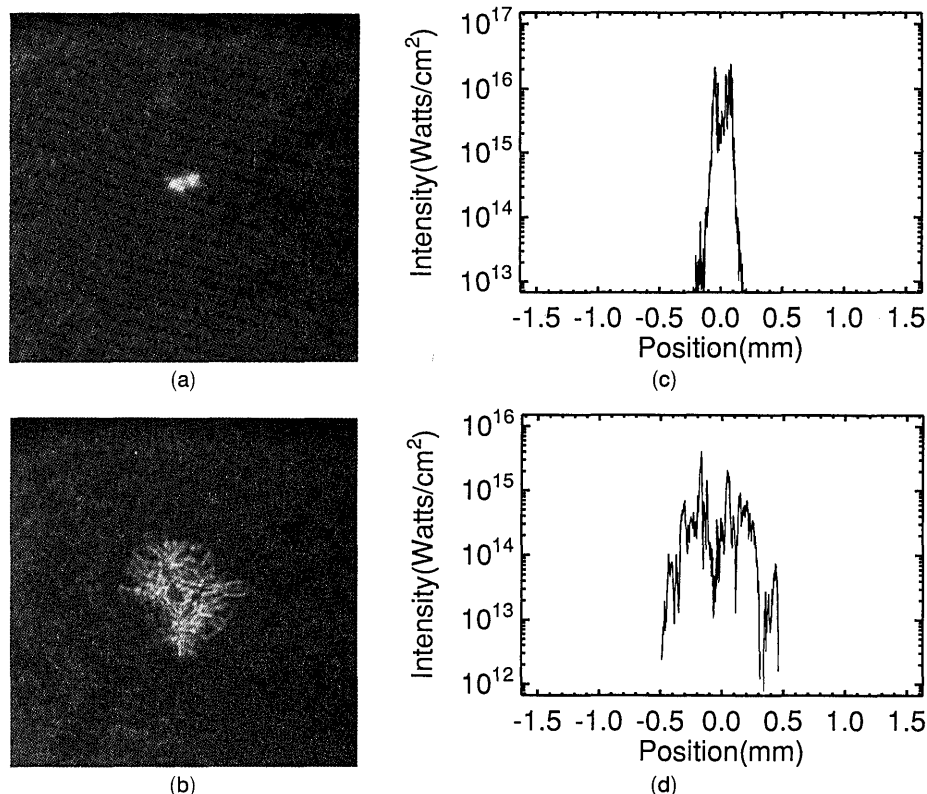
Fig. 10. Photographs of the intensity distributions for the Nova laser operating at 351 nm at (a) best focus and (b) in a plane 4 mm past best focus. The spatial scales are the same for both pictures. Horizontal line scans through the figures of (a) and (b) are shown in (c) and (d), respectively. The intensity values correspond to a 1-TW incident beam power.

the physical step heights and edge definitions. Our RPP's show a lateral edge definition of ~ 15 μm and step heights typically within a few percent of the nominal.

C. Laser Damage Threshold

The laser damage thresholds of our phase plates at both 532 and 355 nm were measured at a pulse width of 10 ns in the Reptile laser damage facility at Lawrence Livermore National Laboratory. The thresholds were nominally 30 J/cm^2 at 532 nm and 12 J/cm^2 at 355 nm. Scaling by the square root of the pulse length, we can calculate damage thresholds of > 9 J/cm^2 at 532 nm and > 3.5 J/cm^2 at 351 nm for the typical 1-ns pulses on Nova. The Nova laser routinely operates at an average fluence of ~ 1 J/cm^2 (for 1-ns pulses) at either 527 nm or 351 nm. Under routine operating conditions, we have not observed any optical damage associated with coating defects.

D. Performance of the Phase Plates on Nova

We fabricated several large-aperture RPP's for use on Nova and also many smaller-aperture (15–20-cm-diameter) RPP's for use on other laser systems by using the sol-gel fabrication procedure discussed in Section 3. The ultimate test of the usefulness of the RPP's is in their effectiveness in homogenizing the beam without producing a coherent spike on axis. As discussed in the introduction, the Nova beam is considerably aberrated because of large apertures and

segmented optics. This leads to an ~ 20-times diffraction-limited focal spot at the harmonic wavelengths. An example of the Nova far-field pattern is shown in Fig. 10(a). For comparison, a picture of the beam 4 mm past best focus is shown in Fig. 10(b), which has a spot size more characteristic of that obtained with phase plates. This data as well as the data with the RPP's shown below were taken in a laser diagnostic station on one arm of the Nova laser that sampled the back-reflected light from a full-aperture beam splitter.[25] It is clear from these pictures that both these patterns are quite nonhomogeneous. The picture in Fig. 10(b) is sufficiently far from focus that the characteristic near-field features
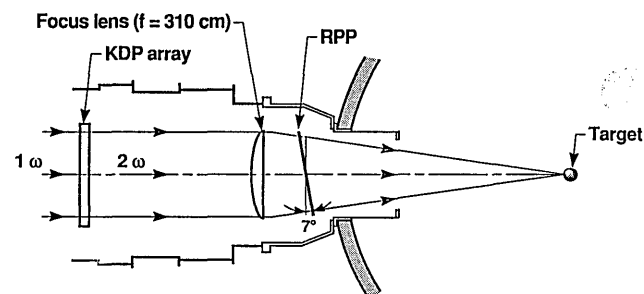

Fig. 11. Schematic illustration of the placement of the RPP on the Nova beam: 1 ω, the fundamental 1.053-μm beam; 2 ω, its second harmonic at 0.527 μm following the conversion through the potassium dihydrogen phosphate (KDP) array.
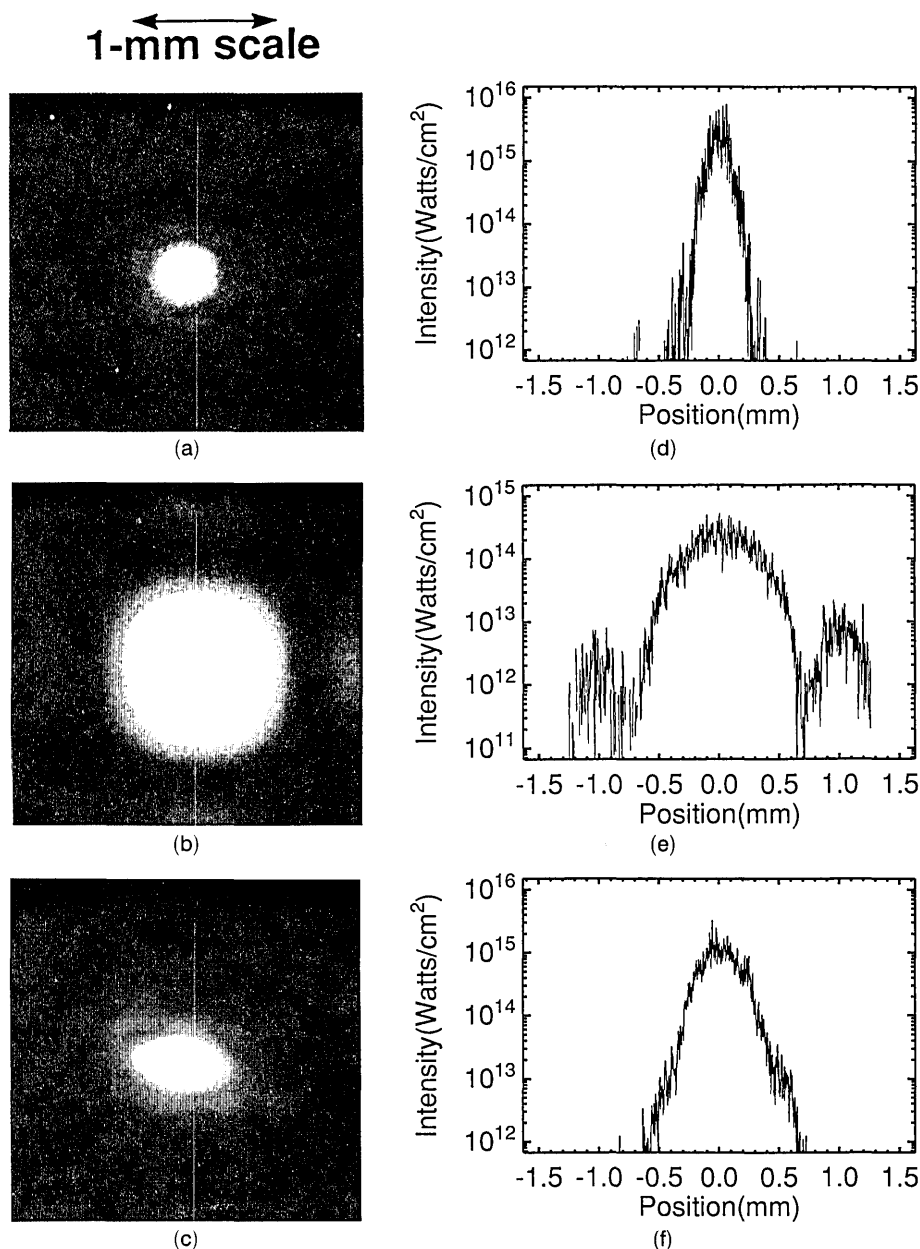
Fig. 12. Photographs of the far-field distributions on Nova with the random phase plates inserted in the beam. For (a), (b), and (c) the sizes of the phase-plate elements and the corresponding operating wavelengths are as follows: (a) 7-mm hexagons (527 nm), (b) 1.3-mm squares (351 nm), (c) stretched hexagons (351 nm). The size of the stretched hexagonal phase-plate element is $h_1 = 3$ mm, $h_2 = 3.4$ mm, and $h_3 = 6.4$ mm. The spatial scale is the same for all three pictures. Horizontal line scans through (a), (b), and (c) are shown in (d), (e), and (f), respectively. The intensity values correspond to a 1-TW incident beam power.

(the central beam block and the segmentation from the frequency conversion array) of the beam are becoming visible.

For homogenizing this pattern, large-aperture RPP's were placed in the Nova beam following the final focus lens, as shown in Fig. 11. The phase plates were installed at this position to avoid any potential damage to downstream optics resulting from the near-field intensity modulations caused by the Fresnel diffraction around the phase step boundaries.[26] The last element (RPP or a plain SiO$_2$ substrate) also acts as a debris shield to protect the focus lens against the target debris and is tilted at 7° to the beam propagation direction to prevent its focusing back-reflection from hitting the frequency conversion array. Because of the placement of the RPP, as shown in Fig. 11, a converging beam is incident on the RPP. For a 70-cm-diameter beam at the lens, this convergence together with the tilt indicates that the effective angle of incidence across the RPP varies from 0° to 14°. The OPD as a function of incidence angle θ between the surface

normal of the RPP and the incident beam is given by

$$\text{OPD} = n_c t \left(1 - \frac{\sin^2\theta}{n_c^2} \right)^{1/2} - t \cos\theta$$

$$\approx (n_c - 1)t \left(1 + \frac{1}{2n_c}\theta^2 \right), \qquad (17)$$

where the approximation is valid for small angles. This equation with $n_c = 1.44$ implies a $\pm 1\%$ variation in the OPD across the Nova aperture. However, this error is not expected to lead to a coherent spike because of beam aberrations, as discussed in Subsection 4.A and below.

The far-field patterns obtained when the regular hexagonal-element, the square-element, and the stretched hexagonal-element random-phase plates are inserted in the Nova beam, as shown in Fig. 12. Introduction of the random phase plate in the beam is seen to completely wash out the Nova beam features is shown in Fig. 10 and to produce a homogeneous far-field pattern characteristic of a single phase-plate element. However, to wash out the Nova features, we need to increase the size of the focal spot. The electric field in the focal plane is a convolution of the far-field patterns for the beam alone and for the RPP. The fine-scale speckle superposed on the far-field envelope of a single phase-plate element is evident. We verified that the experimental intensity distribution of the speckle approximately obeys the expected negative exponential statistics. Deviations from the exponential statistics are observed that arise from remnant beam aberrations and depolarization effects from the vacuum-loaded target focus lens.

We did not observe any coherent spike when the RPP's were fielded on Nova. The full-aperture Nova beam (beam area of ~ 3100 cm^2) illuminates approximately 7300 phase-plate elements on the 7-mm hexagonal RPP (183,400 elements for 1.3-mm squares). Results presented in Fig. 6 would imply that the suppression of the coherent spike for a uniphase beam would require the OPD to be extremely close to $\lambda/2$. However, for non-diffraction-limited beams, the number of elements N in Eq. (13) should be regarded as the number within a uniphase zone. Owing to beam aberrations, the effective number of phase-plate elements illuminated within a nominally uniphase zone on Nova (2–4-cm diameter, estimated from the spot size at best focus) is much smaller than the total number of illuminated elements. This reduction in the number of coherently interfering phase-plate elements permits an increased tolerance on the deviation of the OPD from $\lambda/2$. We found that OPD errors up to 5% from $\lambda/2$ can be tolerated. The permitted error would again be smaller for laser beams with a higher degree of phase uniformity.

5. Summary and Conclusions

We have discussed the characteristics of the far-field intensity distribution caused by a bilevel random phase plate. We then presented in detail a new sol-gel procedure for fabricating large-aperture bilevel random phase plates. Several RPP's ranging from 15 to 80 cm diameter have been fabricated. Our sol-gel process is easy to use and produces a high optical quality, high optical damage threshold product. Finally, we presented experimental data illustrating the effectiveness of RPP's in homogenizing the far-field distribution of the Nova laser.

References and Notes

1. J. Nuckolls, L. Wood, A. Thiessen, and G. Zimmerman, "Laser compression of matter to super-high densities: thermonuclear (CTR) applications," Nature (London) **239**, 139–142 (1972).

2. W. W. Simmons and R. O. Goodwin, "Nova laser fusion facility: design, engineering, and assembly overview," J. Nucl. Technol. Fusion **4**, 8–24 (1983).

3. Y. Kato, K. Mima, N. Miyanaga, S. Arinaga, Y. Kitagawa, M. Nakatsuka, and C. Yamanaka, "Random phasing of high-power lasers for uniform target acceleration and plasma instability suppression," Phys. Rev. Lett. **53**, 1057–1060 (1984).

4. X. Deng, X. Liang, Z. Chen, W. Yu, and R. Ma, "Uniform illumination of large targets using a lens array," Appl. Opt. **25**, 377–381 (1986).

5. R. H. Lehmberg and S. P. Obenschain, "Use of induced spatial incoherence for uniform illumination of laser fusion targets," Opt. Commun. **46**, 27–31 (1983).

6. S. Skupsky, R. W. Short, T. Kessler, R. S. Craxton, S. Letzring, and J. M. Soures, "Improved laser beam uniformity using the angular dispersion of frequency modulated light," J. Appl. Phys. **66**, 3456–3462 (1989).

7. D. Veron, H. Ayral, C. Geouedard, D. Husson, J. Lauriou, O. Martin, B. Meyer, M. Rostaong, and C. Sauteret, "Optical spatial smoothing of Nd:glass laser beam," Opt. Commun. **65**, 42–46 (1988).

8. H. Nakano, K. Tsubakimoto, K. Yagi, T. Jitsuno, M. Nakatuska, S. Nakai, T. Kanabe, and C. Yamanaka, "Irradiation uniformity improvement by incoherence of amplified spontaneous emission in glass laser fusion systems," in *Lasers and Electro-Optics,* Vol. 7 of 1990 OSA Technical Digest Series (Optical Society of America, Washington, D.C., 1990), pp. 280–282.

9. C. N. Danson, R. Bann, D. Pepler, N. Rizvi, I. Ross, T. Afsharrad, S. Coe, M. Dusselberger, and O. Willi, "Focal spot smoothing on the vulcan glass laser system," *1989 OSA Annual Meeting,* Vol. 18 of 1989 OSA Technical Digest Series (Optical Society of America, Washington, D.C., 1989) p. 86.

10. H. T. Powell, S. N. Dixit, and M. A. Henesian, "Beam smoothing capability on the Nova laser," in *Lawrence Livermore National Laboratory ICF Quarterly Report,* Rep. UCRL-

LR-105821-91-1 (Lawrence Livermore National Laboratory, Livermore, Calif., 1990), Vol. 1, pp. 28–38.

11. B. W. Woods, I. M. Thomas, M. A. Henesian, S. N. Dixit, and H. T. Powell, "Large aperture (80-cm diameter) phase plates for beam smoothing on Nova," in *Solid-State Lasers II,* G. Duber, ed., Proc. Soc. Photo-Opt. Instrum. Eng. **1410,** 47–54 (1991).

12. Laboratory for Laser Energetics, "OMEGA phase conversion with distributed phase plates," in *Laboratory for Laser Energetics, Annual Report,* Vol. 33, Q. Rep. DOE/ DP40200-65 (University of Rochester, Rochester, N.Y., 1987), pp. 1–10.

13. C. N. Danson, R. Bann, D. Pepler, I. Ross, J. Exley, D. Hardie, and S. Sails, "Development of random phase plate smoothing technology," in *Rutherford Appleton Laboratory Annual Report RAL-91-025* (Rutherford Appleton Laboratory, Abingdon, UK, 1991), pp. 62–65; M. Desselberger, L. Gizzi, V. Barrow, J. Edwards, F. Khattak, S. Viana, O. Willi, and C. N. Danson, "High-aspect-ratio line focus and plasma production using a random phase plate," Appl. Opt. **31,** 3759–3766 (1992).

14. See the papers in *Diffractive Optics: Design, Fabrication, and Applications,*" in Vol. 9 of 1992 OSA Technical Digest Series (Optical Society of America, Washington, D.C., 1992).

15. B. W. Woods, I. M. Thomas, S. N. Dixit, H. T. Powell, and M. A. Henesian, "Large aperture sol-gel phase plates for beam smoothing on Nova," in *Conference on Lasers and Electro-Optics,* Vol. 12 of 1992 OSA Technical Digest Series (Optical Society of America, Washington, D.C., 1992), p. 456.

16. I. M. Thomas, "High laser damage threshold porous silica antireflective coating," Appl. Opt. **25,** 1481–1483 (1986).

17. J.-L. Nogues, "Pure silica diffraction grating and microlens arrays made by the sol-gel process," in *Diffractive Optics: Design, Fabrication, and Applications,* Vol. 9 of 1992 OSA Technical Digest Series (Optical Society of America, Washington, D.C., 1992), pp. 15–17.

18. J. W. Goodman, *Introduction to Fourier Optics* (McGraw-Hill, New York, 1968), Chap. 5, pp. 85–90.

19. M. Born and E. Wolf, *Principles of Optics,* 6th ed. (Pergamon, New York, 1980), Chap. 8, pp. 393–401.

20. R. E. English, Jr., "Diffraction theory for polygonal apertures," Ph.D. dissertation (University of Rochester, Rochester, N.Y., 1988).

21. J. W. Goodman, "Statistical properties of speckle patterns," in *Laser Speckle and Related Phenomena,* J. C. Dainty, ed. (Springer, New York, 1984), Chap. 2, pp. 9–75.

22. C. J. Brinker and C. W. Scherer, *Sol-Gel Science* (Academic, New York, 1990), Chap. 13.

23. F. Abeles, "Methods for determining optical parameters of thin films," in *Progress in Optics,* E. Wolf, ed. (North-Holland, Amsterdam, 1963), Vol. 2, Chap. 6, pp. 251–288.

24. R. Epstein and S. Skupsky, "Anticipated improvement in laser beam uniformity using distributed phase plates with quasi-random patterns," J. Appl. Phys. **68,** 924–931 (1990).

25. P. J. Wegner and M. A. Henesian, "Precision high-power solid-state laser diagnostics for target-irradiation studies and target plane irradiation modeling," in *Laser Beam Diagnostics,* R. N. Hindy and Y. Kohanzadeh, eds., Proc. Soc. Photo-Opt. Instrum. Eng. **1414,** 162–174 (1991).

26. L. G. Seppala, R. B. Ehrlich, S. N. Dixit, M. A. Henesian, H. T. Powell, P. J. Wegner, and B. W. Woods, "Intense peaks in near-field diffraction from random phase plates," in *Conference on Lasers and Electro-Optics,* Vol. 10 of 1991 OSA Technical Digest Series (Optical Society of America, Washington, D.C., 1991) p. 274.